Energy Conversion and Management 85 (2014) 85–101

Contents lists available at ScienceDirect

Energy Conversion and Management

journal homepage: www.elsevier.com/locate/enconman

Investigation and design optimization of exhaust-based thermoelectric generator system for internal combustion engine

Zhiqiang Niu, Hai Diao, Shuhai Yu, Kui Jiao *, Qing Du, Gequn Shu

State Key Laboratory of Engines, Tianjin University, 92 Weijin Road, Tianjin 300072, China

ARTICLE INFO

Article history:
Received 11 April 2014
Accepted 8 May 2014
Available online 13 June 2014

Keywords:
Thermoelectric generator
Exhaust channel
Waste heat recovery
3-D numerical model

ABSTRACT

Thermoelectric generator (TEG) has attracted considerable attention for the waste heat recovery of internal combustion engine. In this study, a 3-D numerical model for engine exhaust-based thermoelectric generator (ETEG) system is developed. By considering the detailed geometry of thermoelectric generator (TEG) and exhaust channel, the various transport phenomena are investigated, and design optimization suggestions are given. It is found that the exhaust channel size needs to be moderate to balance the heat transfer to TEG modules and pressure drop along channel. Increasing the number of exhaust channels may improve the performance, however, since more space and TEG modules are needed, the system size and cost need to be considered as well. Although only placing bafflers at the channel inlet could increase the heat transfer coefficient for the whole channel, the near wall temperature downstream might decrease significantly, leading to performance degradation of the TEG modules downstream. To ensure effective utilization of hot exhaust gas, the baffler angle needs to be sufficiently large, especially for the downstream locations. Since larger baffler angles increase the pressure drop significantly, it is suggested that variable baffler angles, with the angle increasing along the flow direction, might be a middle course for balancing the heat transfer and pressure drop. A single ETEG design may not be suitable to all the engine operating conditions, and making the number of exhaust channels and baffler angle adjustable according to different engine operating conditions might improve the performance.

1. Introduction

In recent years, the global energy and environmental issues have driven the application of waste heat recovery techniques in main energy conversion devices such as internal combustion engine (ICE). For a typical gasoline engine as an example, only 25% of the chemical energy in fuel can be converted into useful energy for powering vehicles and other devices, and the rest of the energy is discharged to the ambient environment in the form of waste heat through the exhaust and coolant [1]. If 6% of the exhaust heat is converted into electrical energy, it would be possible to reduce the fuel consumption by about 10% [2]. Thus, the technologies of waste heat recovery for ICE become significantly important for improving the overall efficiency and reducing the fuel consumption. Among the different technologies, thermoelectric generator (TEG) has received many attentions due to the advantages such as free maintenance, high reliability and quiet operation.

Many studies have been conducted to use TEG for the waste heat recovery of ICE exhaust. LaGrandeur et al. [3] developed and tested a TEG system based on an in-line six-cylinder gasoline engine in BMW 530I. It was found that the influence of the primary heat exchanger backpressure should not be neglected in high-load operation (e.g. highway driving cycles). Thacher et al. [4] conducted tests of an automobile exhaust TEG system installed in a GMC Sierra pickup. They concluded that the performance of the system is sensitive to the coolant temperature, and the system weight should be considered. Similarly, Hsu et al. [5] tested the performance of a Bi_2Te_3-based TEG system, which is connected to the middle of an exhaust pipe in a Chrysler Neon. Saqr et al. [6] made a comprehensive review of the main aspects of exhaust-based thermoelectric generator (ETEG) in the past 20 years, and summarized the main challenges for ETEG systems such as the need in efficiency improvement.

Beside the above mentioned tests of ETEG systems in vehicles, in-depth investigation and optimization of ETEG system are necessary for performance improvement. Typically, an ETEG system mainly consists of three components: TEG module, exhaust channel and heat sink. Thus, the optimization of an ETEG system mainly has two approaches: one aims at the development of

* Corresponding author. Tel.: +86 22 27404460; fax: +86 22 27383362.
E-mail address: kjiao@tju.edu.cn (K. Jiao).

http://dx.doi.org/10.1016/j.enconman.2014.05.061
0196-8904/

Nomenclature

A	cross section area of inlet and outlet (m^2)
B	fuel consumption rate ($kg\ h^{-1}$)
E	electric field intensity vector ($V\ m^{-1}$)
h	heat transfer coefficient ($W\ m^{-2}\ K^{-1}$)
I	current (A)
J	current density ($A\ m^{-2}$)
k	turbulence kinetic energy ($J\ kg^{-1}$)
L	number of exhaust channel
N	number of bafflers
$\vec{n}$	normal vector of wall
p	pressure (Pa)
P	power (W)
Q	heat (W)
$\dot{S}$	energy source ($W\ m^{-3}$)
T	temperature (K)
u	x-velocity ($m\ s^{-1}$)
V	potential (V)
$\dot{V}$	source term of Seebeck potential ($V\ m^{-2}$)
v	velocity ($m\ s^{-1}$)

Greeks symbols

α	Seebeck coefficient ($V\ K^{-1}$)
β	angle between bafflers and bottom wall of exhaust channel (°)
ε	turbulent dissipation rate ($m^{-2}\ s^{-3}$)
η	efficiency (%)
λ	thermal conductivity ($W\ m^{-1}\ K^{-1}$)
μ	effective turbulent viscosity (Pa s)
ρ	density ($kg\ m^{-3}$)
σ	electrical conductivity ($S\ m^{-1}$)

Subscripts/superscripts

1	normal vector 1
2	normal vector 2
c	cold side
c,s	ceramic, stainless steel
copper	copper unit
eff	effective
ext	exhaust gas
ε	turbulence kinetic energy dissipation
h	hot side
ICE	internal combustion engine
i	direction of x coordinate
in	inlet
j	direction of y coordinate
k	turbulence kinetic energy
l	loss
n	n unit
n	net
o	Ohmic voltage
out	output voltage
ohm	Ohmic potential
p	p unit
red	reduction of fuel
s	Seebeck voltage
sbk	Seebeck potential
T	temperature
TEG	thermoelectric generator
wb	bottom wall of TEG modules
wi	inner wall of exhaust channel

high-efficiency thermoelectric materials and the design of TEG structures (e.g. segmented TEG modules) [7–14]; and the other is mainly to enhance the heat transfer from heat source to TEG and from TEG to heat sink [15–17]. Numerous experiments have been conducted to investigate the key factors that influence the performance of ETEG system following these two approaches. For example, new exhaust channel designs were proposed. Lesage et al. [18] placed spiral and panel inserts in exhaust channels to experimentally investigate their effect on the performance of TEG. In the experiment of Rezania [19], a heat exchanger with 20 micro-channels in the heat sink was tested for the performance improvement of TEG.

To gain deep insights of the transport phenomena in TEG systems, theoretical and numerical models have been developed by researchers. The one-dimensional (1-D) numerical model of Chen et al. [20] considered the variable material properties, and this model was further extended to a three-dimensional (3-D) numerical model [21]. Besides, two approaches for developing 3-D TEG models were proposed in [22]. Except the 3-D models for single TEG units [21,22], Rowe and Gao [23] developed a 1-D

Table 1
Four typical operating conditions of the diesel engine considered in this study [28].

Parameters	Case 1	Case 2 (base)	Case 3	Case 4
Power output (kW)	258.3	235.8	176.2	117.7
Fuel consumption rate ($kg\ h^{-1}$)	53.22	47.79	35.43	23.91
Temperature of exhaust gas (K)	808.15	792.15	747.15	693.15
Mass flow rate of exhaust gas ($kg\ s^{-1}$)	0.2981	0.2752	0.2235	0.1697
Output temperature of jacket water (K)	366.15	365.65	364.65	363.75
Mass flow rate of jacket water ($kg\ s^{-1}$)	2.1	2.1	2.1	2.1

Table 2
Properties of air [29].

Temperature, T (K)	Density, ρ ($kg\ m^{-3}$)	Specific heat, c_p ($kJ\ kg^{-1}\ K^{-1}$)	Viscosity, μ (Pa s)	Thermal conductivity, k ($W\ m^{-1}\ K^{-1}$)
600	0.580	1.051	3.06×10^{-5}	0.0466
800	0.441	1.099	3.65×10^{-5}	0.0557
1000	0.348	1.141	4.24×10^{-5}	0.0681

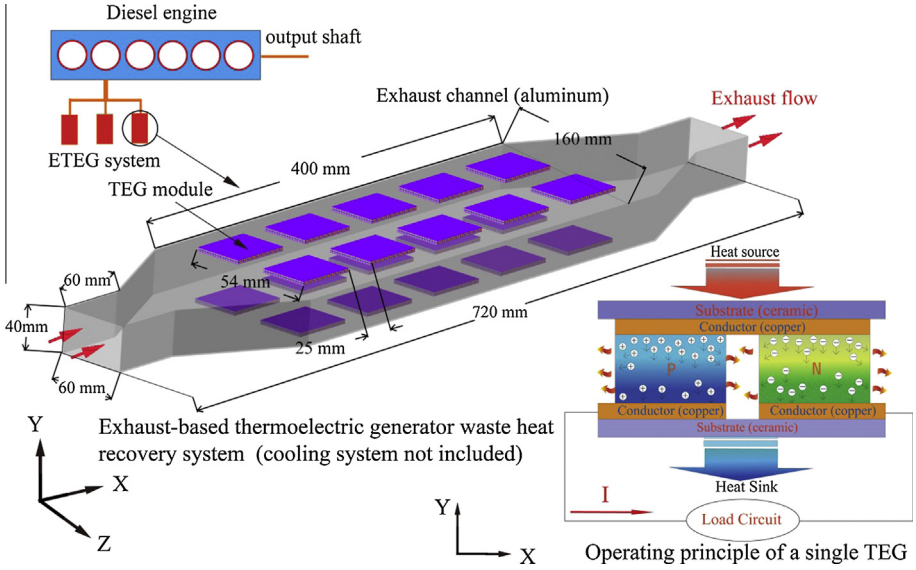

Fig. 1. Schematic of the exhaust-based thermoelectric generator (ETEG) system for a diesel engine.

Table 3
Design parameters of a single TEG unit.

Parameters	p/n semiconductors		Copper	Ceramic	Stainless steel	References
Seebeck coefficient ($V\ K^{-1}$)	Constant	$\pm 2.2 \times 10^{-4}$	–	–	–	[15]
	Variable	$\pm(2224 + 930.6 * T - 0.9905 * T^2) \times 10^{-9}$ (300 K – 500 K, T in K)			–	[32]
Thermal conductivity ($W\ m^{-1}\ K^{-1}$)	Constant	1.5	350	36	14.99	[15,31,32]
	Variable	$(62{,}605 - 277.7 * T + 0.4131 * T^2) \times 10^{-4}$ (300 K – 500 K, T in K)				[32]
Electrical conductivity ($S\ m^{-1}$)	Constant	1.0×10^5	5.9×10^7	–	–	[15]
	Variable	$(5112 + 163.4 * T + 0.6279 * T^2)^{-1} \times 10^{10}$ (300 K – 500 K, T in K)				[32]
Cross section area (mm^2)	2×2		5.2×2	5.2×2	–	–
Thickness (mm)	1.25		0.5	0.635	1	–

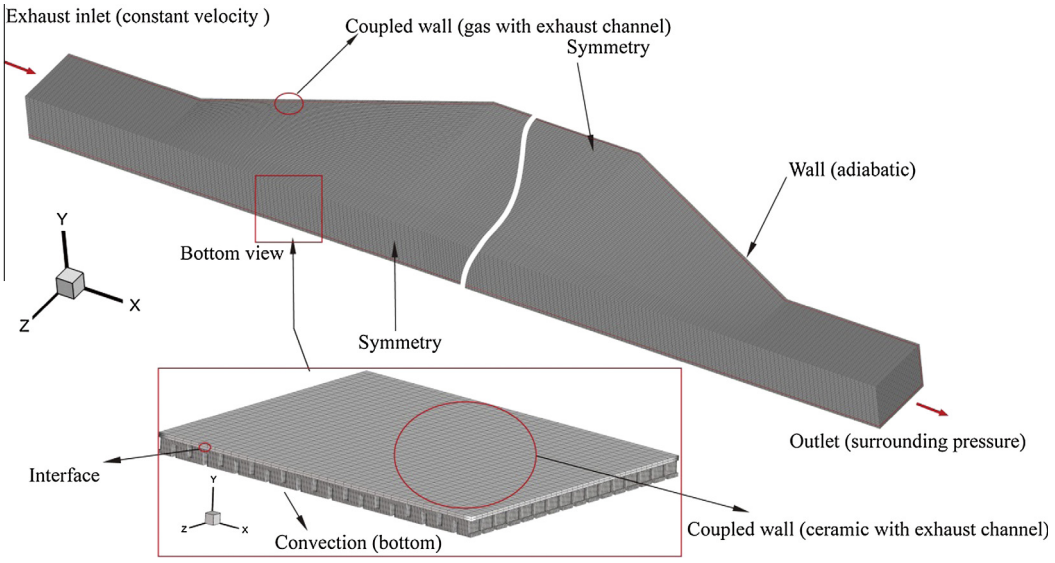

Fig. 2. Computational domain and mesh.

model to assess the performance of TEG modules (a TEG module includes many TEG units). Similarly, other 1-D models for TEG modules were also developed [24–26].

To investigate more detailed transport phenomena, such as the 3-D fluid flow in heat source or heat sink and the temperature distribution in TEG units, 3-D numerical models are needed, and yet,

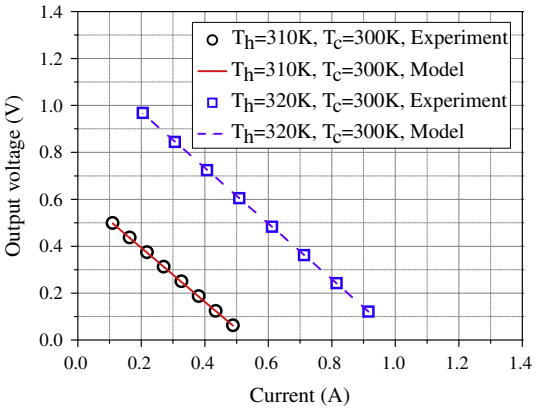

Fig. 3. Comparison of the experimental data in [36] and simulation results [22].

Table 4
Simulation cases.

Parameters	Specifications
Cross section of inlet and outlet, A (mm^2)	30 × 40, 60 × 40, 120 × 40
Number of exhaust channel, L	1, 2, 3
Number of bafflers, N	0, 1, 2, 3, 4, 5, 6
Angle of baffler, β (°)	10°, 20°, 30°, 40°
Operating conditions of ICE	Cases 1–4 of Table 1

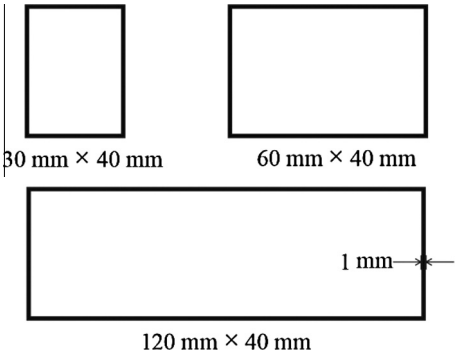

Fig. 4. Different inlet/outlet cross sections of exhaust channel.

few works developed 3-D numerical models for ETEG systems. Zhou et al. [15] incorporated water-fed heat exchangers with parallel and counter flow designs in their TEG model, and discussed the effect of heat exchanger design on performance. Weng et al. [27] developed a 3-D exhaust channel model with a 1-D TEG model to predict the output power of ETEG system. To the best of the authors' knowledge, full 3-D numerical model for ETEG system with exhaust channel and TEG modules were rarely developed.

In this study, a 3-D numerical model for ETEG system of ICE is developed. In the numerical simulations, the effect of the exhaust channel size on the overall performance of ETEG system is investigated. Bafflers are also installed in the exhaust channel at different locations and with different orientations, and its influence on the output power of ETEG and pressure drop along channel under different operating conditions is discussed in details.

2. Model development

The ICE considered in this study is an in-line six-cylinder turbocharged diesel engine, and the operating parameters of this

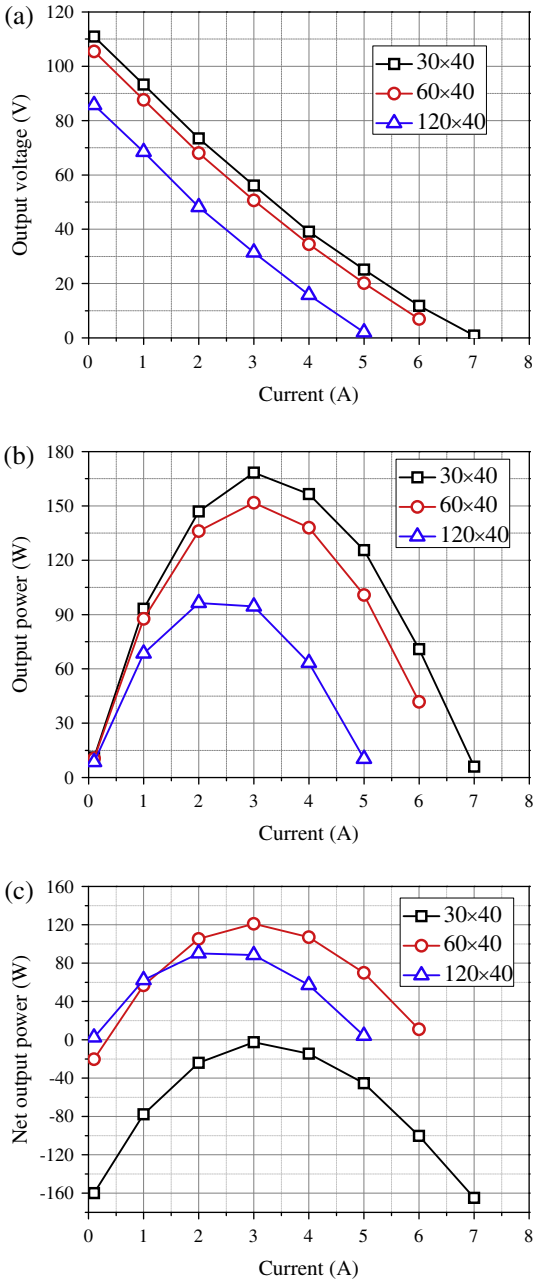

Fig. 5. Change of output voltage (a), power (b) and net power (c) with current for the ETEG systems with different exhaust inlet/outlet cross sections.

Table 5
Pressure drop and power loss through the exhaust channels with three different inlet/outlet cross sections.

Cross section (mm × mm)	Pressure drop Δp (Pa)	Inlet velocity v_{in}(m s^{-1})	Inlet area A (mm^2)	Power loss P_l (W)
30 × 40	1643.0	97.8	1064	171.0
60 × 40	296.4	47.2	2204	30.8
120 × 40	59.1	23.2	4484	6.1

engine are given in Table 1 [28]. Note that the power output defined in Table 1 is the actual power measured by dynamometer. The output temperature of jacket water is measured at the engine outlet, which is considered to be the inlet condition of the cold side of the ETEG system. Based on the mass flow rate of jacket water

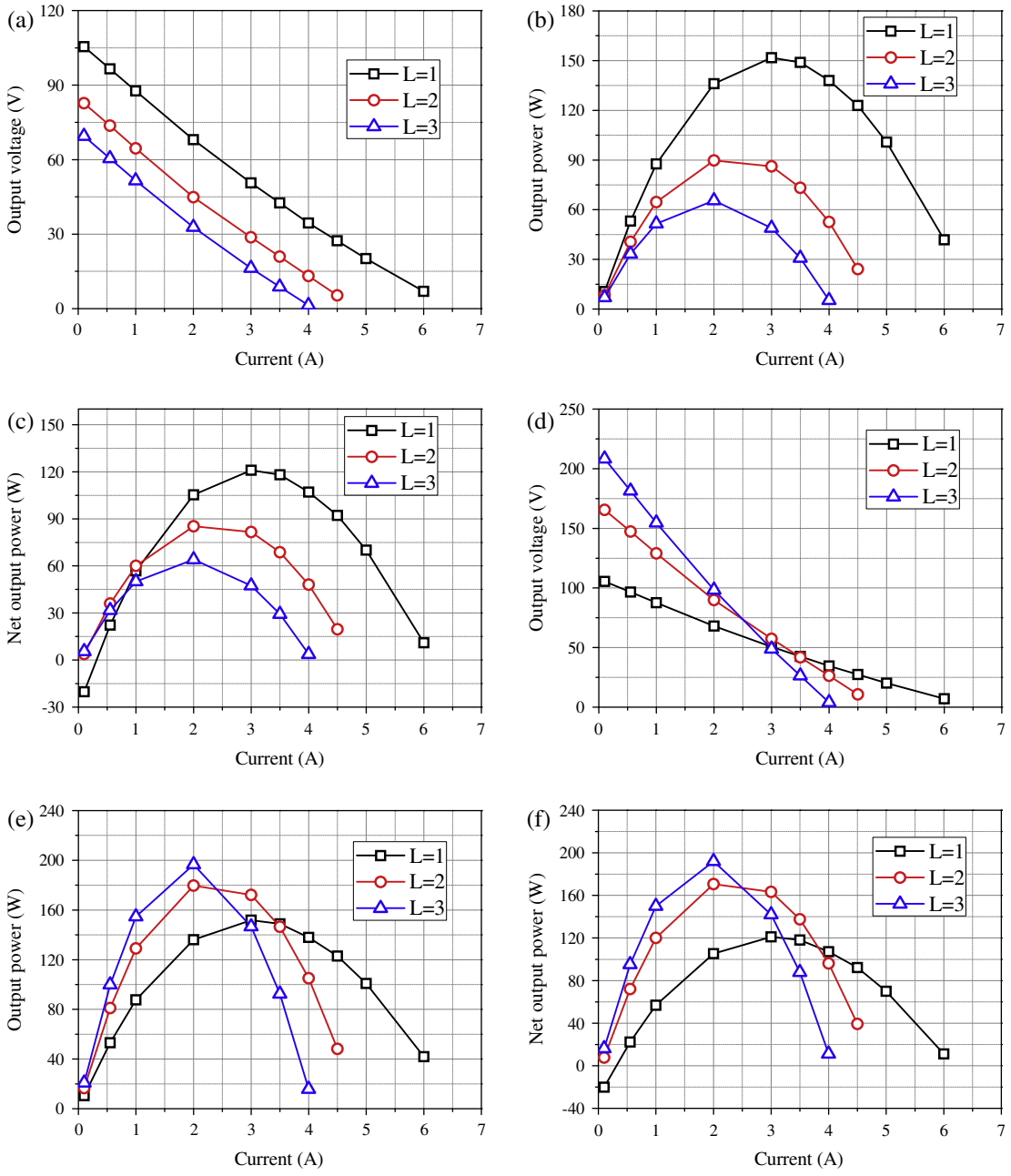

Fig. 6. Change of output voltage per exhaust channel (a), power per exhaust channel (b), net power per exhaust channel (c), voltage of all exhaust channel(s) (d), power of all exhaust channel(s) (e), and net power of all exhaust channel(s) (f) with current for the ETEG systems with different numbers of exhaust channels per cylinder (L = 1, 2, 3).

Table 6
Pressure drop and power loss through exhaust channels with different numbers of exhaust channels for one cylinder of the six-cylinder engine.

Number of channels L	Inlet velocity v_{in}(m s^{-1})	Pressure drop per channel Δp (Pa)	Power loss per channel P_l (W)	Power loss in all channels $L \cdot P_l$ (W)
1	47.2	296.4	30.8	30.8
2	22.9	88.7	4.5	8.9
3	15.3	45.0	1.5	4.6

and the heat transfer rate from TEG to jacket water, it can be estimated that the temperature of jacket water may increase by about 3–5 K by flowing through the ETEG system considered in this study. After that, since the jacket water still needs to be cooled down through radiators before entering the engine again, such slight temperature increment of jacket water is assumed to have negligible effect on the engine. Properties of air are used for the engine exhaust for consistent comparison of the different simulation cases, as given Table 2 [29], because the exact exhaust components under different operating conditions are unknown, and it was recommended that the error associated with using air properties for exhaust is usually less than 2% [30].

A schematic of the ETEG system (with empty exhaust channel) is shown in Fig. 1. Since high flow rates in exhaust channel may cause large pressure drops, the exhaust channel shown in this figure only provides the flow path of the exhaust from one cylinder, corresponding to one-sixth of the exhaust flow of the six-cylinder engine; and to further decrease the pressure drop,

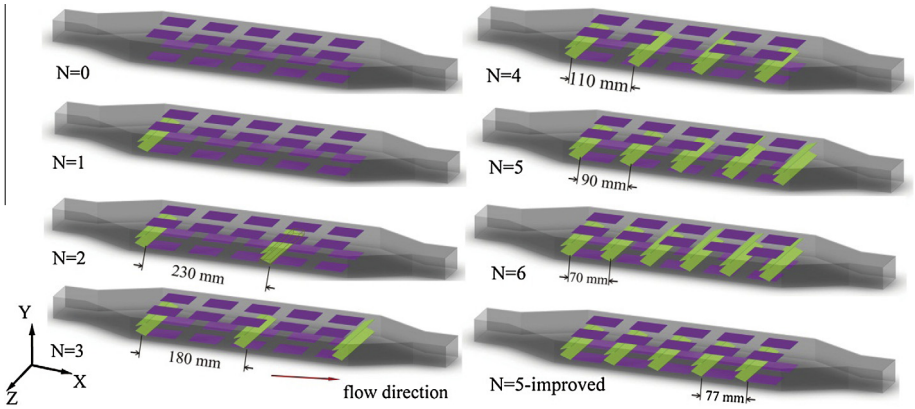

Fig. 7. Schematic of the exhaust channels with different numbers of bafflers (N).

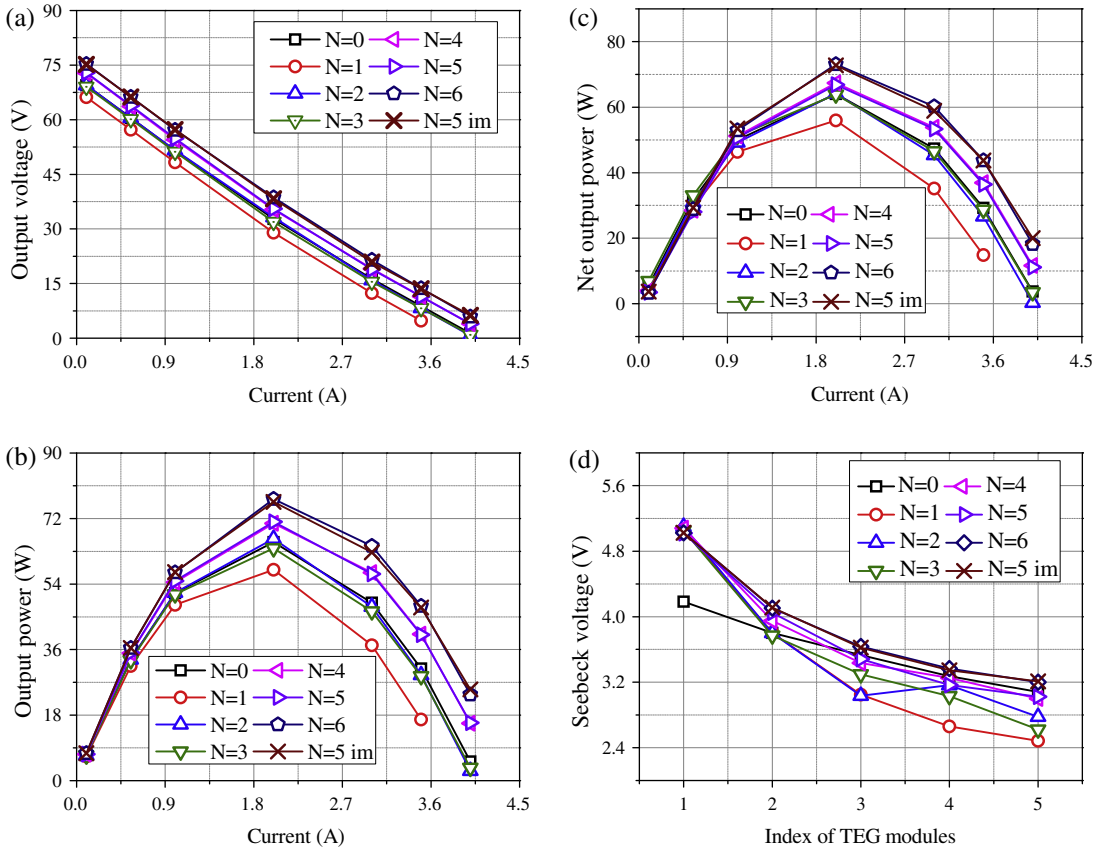

Fig. 8. Change of output voltage (a), power (b) and net power (c) with current, and Seebeck voltages of different TEG modules at 0.1 A (d) for the ETEG systems with different numbers of bafflers.

Table 7
Ranges of X-coordinate for the five TEG modules shown in Fig. 2.

Index of TEG module	1	2	3	4	5
Range of X-coordinate (mm)	−0.3 to 51.7	76.7 to 128.7	153.7 to 205.7	230.7 to 282.7	307.7 to 359.7

the cases with two and three exhaust channels for one cylinder are also investigated. Details of the flow rate and channel size effect are discussed in Section 3. Because of the same operating

Table 8
Pressure drop and power loss through exhaust channels with different numbers of bafflers.

Number of bafflers	Pressure drop Δp (Pa)	Power loss P_l (W)
$N = 0$	45.0	1.5
$N = 1$	58.1	2.0
$N = 2$	70.3	2.4
$N = 3$	82.4	2.8
$N = 4$	98.1	3.3
$N = 5$	113.0	3.8
$N = 6$	126.1	4.3
$N = 5$ im	113.4	3.8

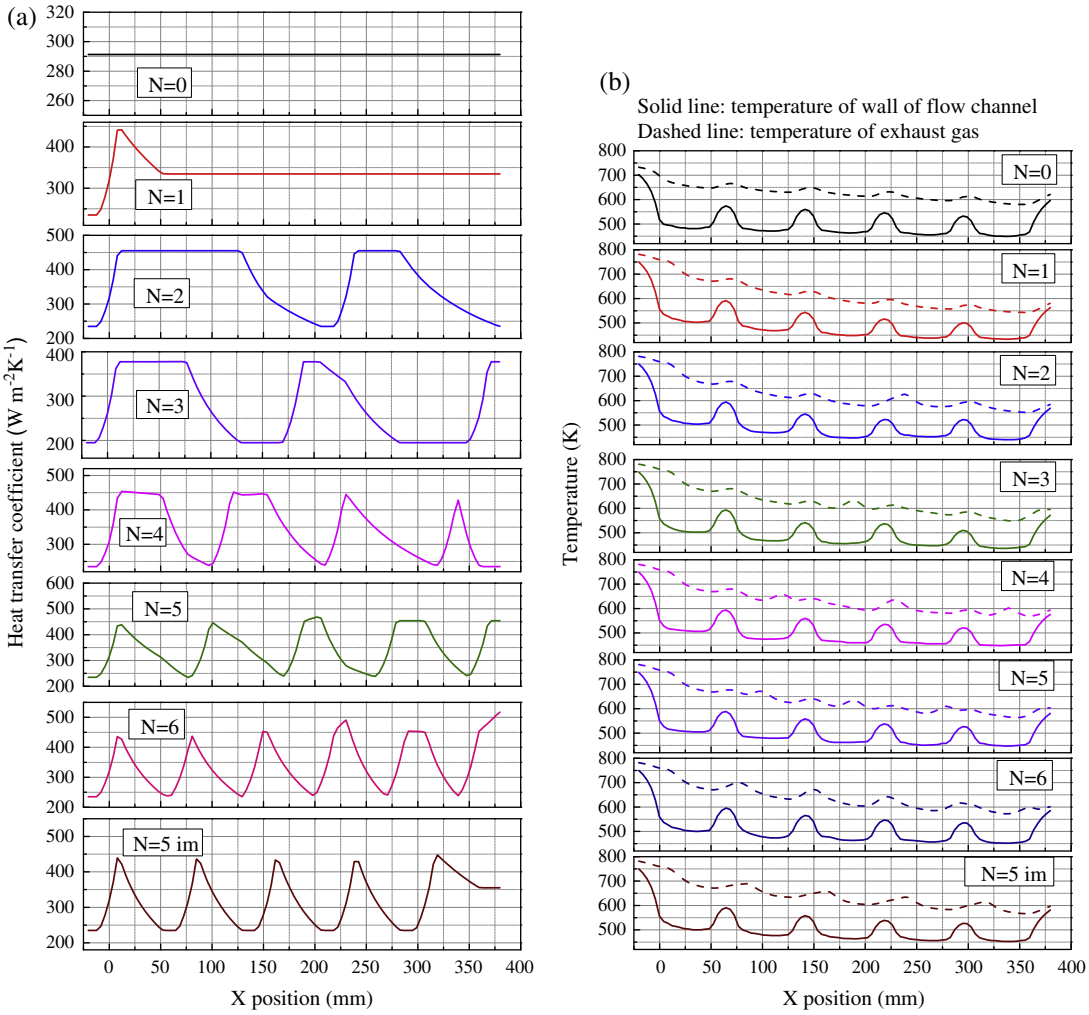

Fig. 9. Heat transfer coefficient (a) and temperatures of gas (middle of exhaust channel and 1 mm from channel wall) and wall (middle of exhaust channel) (b) along the flow direction (*X*-direction) in exhaust channel with different numbers of bafflers.

conditions of the six cylinders, only one exhaust channel with TEG modules is considered in this study.

The shell of the exhaust channel is stainless steel 310 with a thickness of 1 mm. 20 TEG modules are placed on the surface of exhaust channel to be heated, and the cooling water of the engine is used as the heat sink (not shown in Fig. 1). A TEG module includes 160 TEG units. These units are electrically connected in series, therefore they have the same electrical current. On the other hand, these units share the same heat source and heat sink, and heat transfers through them simultaneously, meaning that they are thermally connected in parallel. The dimensions of an assembled TEG module are 41 mm × 26 mm × 3.52 mm. A single TEG unit includes a p-type semiconductor and an n-type semiconductor, and they are connected with a conductor (e.g. copper). The insulation of the TEG units is achieved by placing substrates (e.g. ceramic) on the top and bottom sides, as shown in Fig. 1. The design parameters of a single TEG unit are given in Table 3 [15,31,32].

In this study, the thermoelectric material considered is bismuth telluride (Bi_2Te_3), as shown in Table 3, both the constant and variable properties of the thermoelectric (p/n semiconductors) materials are considered. The numeral simulations consume significant computational time, and it saves about 80% of the computational time if constant properties are used for the thermoelectric materials. Besides, the simulations in Sections 3.1–3.4 only investigate the exhaust channel design effect with the same heat source and heat sink conditions, therefore, the constant material properties are considered in these sections under the same engine operating condition (Case 2 in Table 1). For the simulations with variable engine operating conditions (Cases 1–4 in Table 1) in Section 3.5, since the heat source and heat sink change, the variable material properties are used.

2.1. Conservation equations for exhaust channel

The conservation equations of mass, momentum and energy for the steady-state flow in exhaust channel are

$$\nabla \cdot \vec{v} = 0 \tag{1}$$

$$\nabla \cdot (\vec{v}\vec{v}) = -\frac{1}{\rho}\nabla p + \nabla \cdot (\nu \nabla \vec{v}) \tag{2}$$

$$\nabla \cdot (\vec{v} T_{ext}) = \nabla \cdot (\lambda_{ext} \nabla T_{ext}) \tag{3}$$

In this study, the Reynolds number ranges from 6000 to 38,000 in the exhaust channel, and the renormalization group (RNG) $k-\varepsilon$ turbulence model is used:

$$\frac{\partial}{\partial x_i}(\rho k u_i) = \frac{\partial}{\partial x_j}\left(a_k \mu_{eff} \frac{\partial k}{\partial x_j}\right) + G_k + G_b - \rho\varepsilon \tag{4}$$

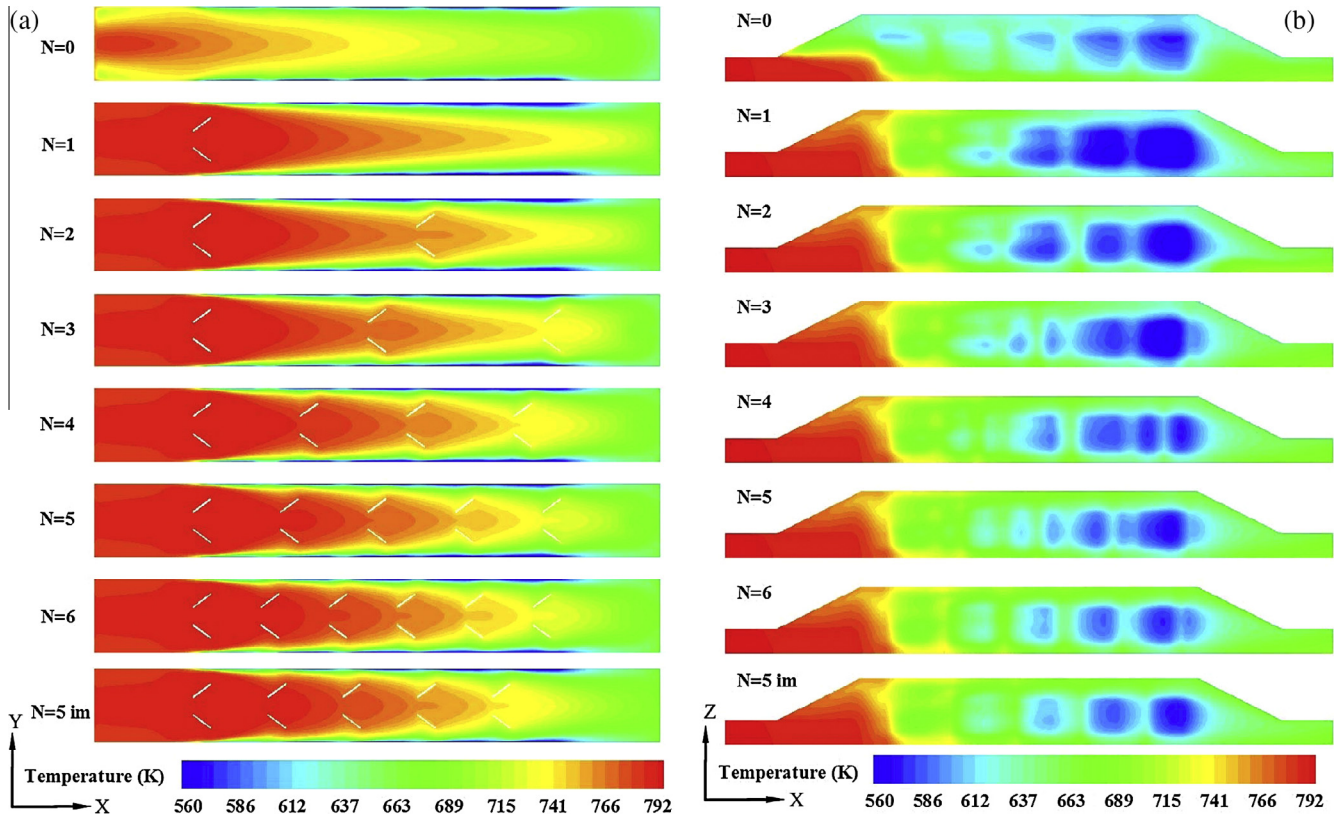

Fig. 10. Contours of temperature in the middle planes of the exhaust channels (a), and near the channel walls (only half wall is shown) with TEG modules (b) for different numbers of bafflers.

$$\frac{\partial}{\partial x_i}(\rho\varepsilon u_i) = \frac{\partial}{\partial x_j}\left(a_\varepsilon \mu_{eff}\frac{\partial \varepsilon}{\partial x_j}\right) + C_{1\varepsilon}\frac{\varepsilon}{k}(G_k + C_{3\varepsilon}G_b) - C_{2\varepsilon}\rho\frac{\varepsilon^2}{k} - R_\varepsilon \tag{5}$$

where G_k is the turbulence kinetic energy generation due to mean velocity gradient. G_b is the turbulence kinetic energy generation due to buoyancy. a_k and a_ε are the inverse effective Prandtl numbers for k and ε. More details of the formulation can be found in [33].

2.2. Conservation equations for thermoelectric generator

The steady-state energy conservation equation in TEG is

$$\nabla\cdot\left[\lambda_{p,n,copper}\nabla T_{p,n,copper}\right] + \dot{S}_T = 0 \tag{6}$$

where $\lambda_{p,n,copper}$ (W m^{-1} K^{-1}) is the thermal conductivity of p-type, n-type and copper units. $T_{p,n,copper}$ (K) is the temperature of p-type, n-type and copper units. $\dot{S}_T$ (W m^{-3}) represents the energy source such as Joule heat and Thomson heat generated in TEG:

$$\dot{S}_T = \begin{cases} \frac{1}{\sigma_p}J_p^2 - \nabla\alpha_p T_p J_p; & \text{p-type unit} \\ \frac{1}{\sigma_n}J_n^2 - \nabla\alpha_n T_n J_n; & \text{n-type unit} \\ \frac{1}{\sigma_{copper}}J_{copper}^2; & \text{copper units} \end{cases} \tag{7}$$

where $J_{p,n,copper}$ (A m^{-2}) is the electrical current intensity vector, and $\sigma_{p,n,copper}$ (S m^{-1}) is the electrical conductivity.

The energy conservation equation in ceramic and stainless steel 310 in steady state only accounts for the heat conduction:

$$\nabla\cdot(\lambda_{c,s}\nabla T_{c,s}) = 0 \tag{8}$$

where $\lambda_{c,s}$ (W m^{-1} K^{-1}) is the thermal conductivity of ceramic and stainless steel units.

The balance of electrical motive force due to Seebeck effect in p/n units is written as

$$\nabla V_{sbk} = -\alpha_{p,n}\nabla T \tag{9}$$

where V_{sbk} (V) is the Seebeck potential, and $\alpha_{p,n}$ (V K^{-1}) is the Seebeck coefficient of p/n units. Taking the divergence of V_{sbk}, Eq. (9) yields:

$$\nabla\cdot(-\nabla V_{sbk}) + \dot{V}_{sbk} = 0 \tag{10}$$

where $\dot{V}_{sbk}$ (V m^{-2}) is the source term:

$$\dot{V}_{sbk} = \begin{cases} \nabla\cdot\left[-\alpha_p\nabla T_p\right]; & \text{p-type unit} \\ \nabla\cdot\left[-\alpha_n\nabla T_n\right]; & \text{n-type unit} \end{cases} \tag{11}$$

The Ohmic voltage drop due to the current flow is

$$\nabla V_{ohm} = -\rho_{p,n,copper}J_{p,n,copper} \tag{12}$$

Based on the continuity of current, i.e. $\nabla\cdot J_{p,n,copper} = 0$, Eq. (12) is written as

$$\nabla\cdot\left[-\sigma_{p,n,copper}\nabla V_{ohm}\right] = 0 \tag{13}$$

2.3. Boundary conditions for exhaust channel

At the inlet of exhaust channel, the temperature and velocity of exhaust are defined; and at the outlet, the pressure is fixed at 1 atm. Due to the symmetrical geometry of the exhaust channel, a quarter of the channel is considered as the computational domain with symmetry boundary conditions, as shown in Fig. 2. At the gas–solid interface in the exhaust channel, a coupled thermal boundary condition, without temperature jump at the interface and satisfying the conservation of heat flux, is defined:

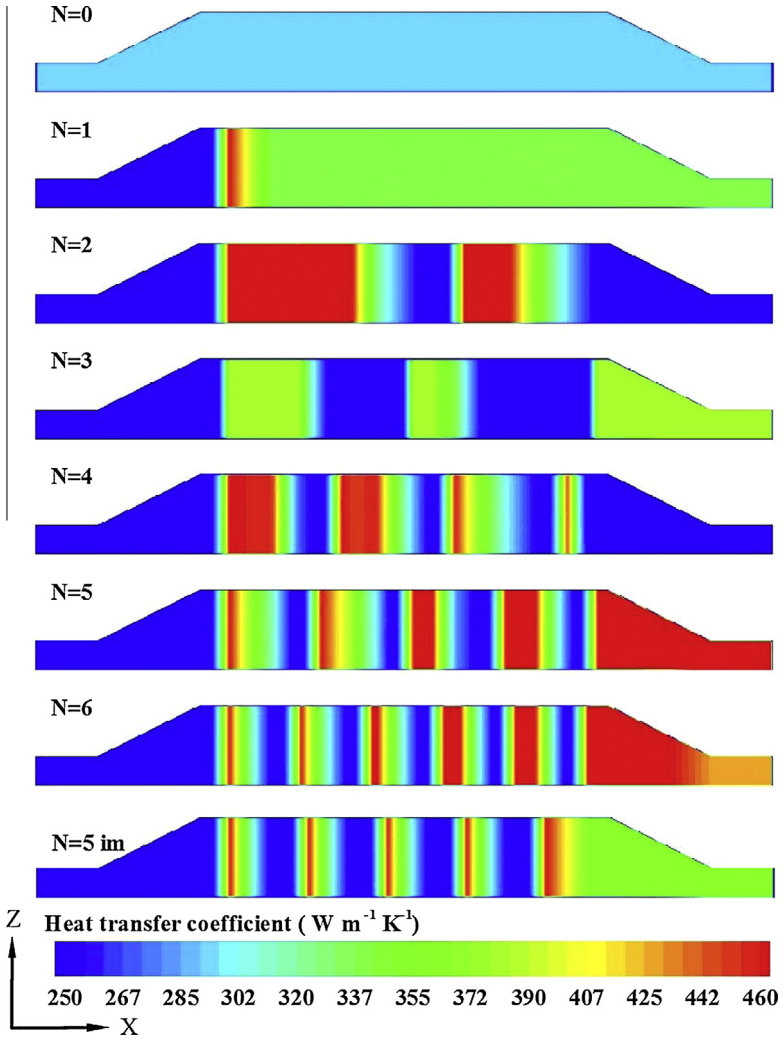

Fig. 11. Contour of heat transfer coefficient for the exhaust channel walls (only half wall is shown) with TEG modules for different numbers of bafflers.

$$h_h(T_{ext} - T_{wi}) = \left(\lambda_s \frac{\partial T_{wi}}{\partial \vec{n}_1}\right)_{wi} \quad (14)$$

where h_h (W m^{-2} K^{-1}) is the heat transfer coefficient between exhaust and wall of exhaust channel. $\vec{n}_1$ is the normal vector to the interface. T_{ext} (K) is the temperature of exhaust, T_{wi} (K) is the temperature at the interface, and λ_s (W m^{-1} K^{-1}) is the thermal conductivity of the channel shell. The heat loss of the exhaust through the other channel walls is neglected in this study. At the interface between exhaust channel shell and TEG module, it also satisfies that the temperate is continuous and the heat flux is conserved.

2.4. Boundary conditions for thermoelectric generator

A constant heat transfer coefficient (h_c, 1000 W m^{-2} K^{-1}) is defined on the cold side of TEG modules representing the engine coolant cooling effect, which is estimated using the Gnielinski equation [34] and was also used in previous TEG models (e.g. [35]). The heat flux to the heat sink is calculated as

$$h_c(T_{wb} - T_c) = \left(\lambda_c \frac{\partial T_{wb}}{\partial \vec{n}_2}\right)_{wb} \quad (15)$$

where h_c (W m^{-2} K^{-1}) is the heat transfer coefficient between heat sink and cold side of TEG modules; $\vec{n}_2$ is the normal vector of the interface of ceramic and heat sink, which points at heat sink; T_{wb} (K) is the wall temperature of cold side of TEG modules; T_c (K) is the temperature of heat sink; and λ_c (W m^{-1} K^{-1}) is the thermal conductivity of cold side of TEG modules, i.e. ceramic.

As mentioned previously, a TEG module includes a number of single TEG units, and the TEG units are connected thermally in parallel and electrically in series. Therefore, all the TEG units have the same operating current. In each TEG unit, for the Ohmic potential, the operating current density and a reference potential of zero are defined at the two ends of the copper conductors, respectively; for the Seebeck potential, an electric field intensity vector and a reference potential of zero are defined at the two ends of the p or n units, respectively. The electric field intensity vector, E (V m^{-1}), is defined as

$$E = \alpha_{p,n} \nabla T_{p,n} \quad (16)$$

The details of the single TEG unit model can also be found in [22]. The output voltage of a TEG module is the summation of the Seebeck voltage and the Ohmic voltage drop of all TEG units in the module:

$$V_{out} = \sum V_s + \sum V_o \quad (17)$$

where V_{out} (V) is the output voltage of a TEG module, V_s (V) is the Seebeck voltage of a single TEG unit, and V_o (V) is the Ohmic voltage drop of a single TEG unit.

2.5. Numerical methods

This numerical model is implemented in the computational fluid dynamics software FLUENT by using its user defined functions to customize the formulation. The individual variables of the conservation equations are solved by using pressure-based segregated solver. The second order upwind method is used for spatial discretization. An algebraic multigrid (AMG) method with a Gauss–Seidel type smoother is used to accelerate the convergence. The computational domain and mesh with some of the boundary conditions are illustrated in Fig. 2. The grid independency study carried out indicates that 4,118,400 cells for five TEG modules and 2,059,680 cells for one exhaust channel are sufficient.

3. Results and discussion

The TEG modeling results have been compared with the experimental data in [36] previously [22], with reasonable agreement, as shown in Fig. 3. It should be noticed that since the current changes almost linearly with voltage, the slope of the curve is mainly determined by the electrical resistance, and the magnitude is mainly determined by the temperature difference (mainly depends on the thermal resistance) and Seebeck coefficient. Therefore, with fixed material properties, by properly considering the electrical and thermal contact resistances at the interfaces between different materials, it is possible to have good agreement between modeling and experimental results. In this study, the exhaust channel is considered with a large number of TEGs in the simulations representing practical 3-D ETEG system. The simulation cases are summarized in Table 4. Three cross-section areas of inlet and outlet, A (m^2), are compared first. Then, the effect of number of exhaust channels corresponding to one cylinder of the six-cylinder engine, L, is tested. After that, bafflers are mounted in the exhaust channel to enhance the performance of ETEG. The influence of number of bafflers, N, is investigated, and an improved exhaust channel design is proposed. The cases with different angles between baffler and inner wall of exhaust channel, β (°), are also simulated for design optimization. Finally, to assess the performance of ETEG under the different operating conditions of the ICE, the four operating conditions given in Table 1 are simulated and compared.

3.1. Effect of exhaust channel inlet/outlet area

Three inlet/outlet cross-section areas of exhaust channel are compared in this section, as shown in Fig. 4 and Table 4. The only difference among the three cross sections is the width, and for

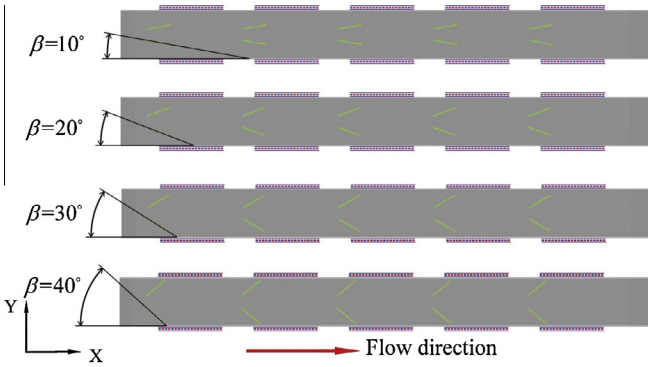

Fig. 13. Schematic of different baffler angles (β).

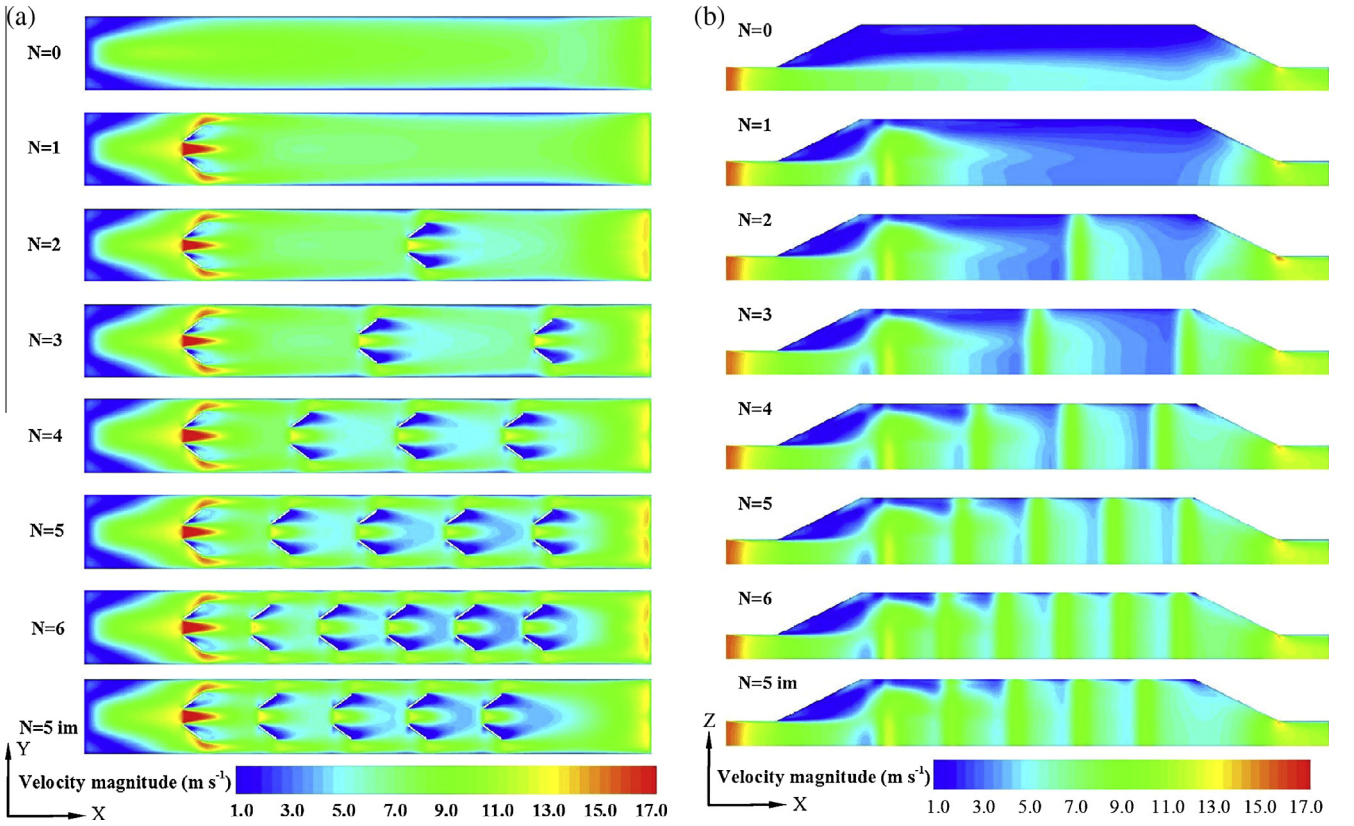

Fig. 12. Contours of velocity magnitude in the middle planes of the exhaust channels (a), and near the channel walls (only half wall is shown) with TEG modules (b) for different numbers of bafflers.

consistent comparison, all the other design and operating parameters are kept the same. For this section, one exhaust channel is considered for one cylinder of the six-cylinder engine.

The voltage, power and net power outputs at different currents of the TEGs are shown in Fig. 5a–c. It should be noticed that the current–voltage and current-power curves in this study are all obtained from numerical simulations in steady-state operating conditions and with the same numerical methods, therefore the numerical results are all repeatable. The statistical error is neglected in the numerical simulations, which is also common in previous numerical models (e.g. [27,28]). This is different from experimental measurements, in which the measured values in different experiments may change, and the statistical error needs to be considered. For all the three designs, the output voltage decreases almost linearly with the increment of current, and the power and net power follow the increasing–decreasing trend. Note that the net power is the TEG output power minus the power loss of exhaust through the channel. The power loss P_l (W) caused by the pressure drop ΔP (Pa) from inlet to outlet is calculated as

$$P_l = \Delta p \cdot A \cdot v_{in} \tag{18}$$

$$P_n = P_o - P_l \tag{19}$$

where A (m^2) is the cross-section area of inlet/outlet, v_{in} ($m\ s^{-1}$) is the velocity of exhaust at inlet, P_n (W) is the net output power, and P_o (W) is the TEG output power.

The pressure or power loss in exhaust channel may affect the engine operation, and the recovery of such power loss requires additional pumping power. Therefore, the net power output could better reflect the overall ETEG performance than the TEG power output.

With the smallest cross section of 30 mm × 40 mm, the voltage and power are the highest (Fig. 5a and b). Taking 3 A as an example, the output voltages the TEGs with cross sections of 30 mm × 40 mm, 60 mm × 40 mm and 120 mm × 40 mm are 56.1 V, 50.6 V and 31.5 V, respectively. The reason is that with the same exhaust mass flow rate, a smaller cross section increases the flow velocity, leading to enhanced heat transfer to the TEGs.

However, in considering the power loss and pressure drop through exhaust channel (Table 5), the exhaust channel with the smallest cross section of 30 mm × 40 mm has the largest pressure drop, about six times that with the cross section of 60 mm × 40 mm, and 28 times that of the cross section of 120 mm × 40 mm, due to the high flow velocity in the small cross sections. As a result, the net power of the ETEG with the smallest cross section of 30 mm × 40 mm is the lowest, and the TEG output power cannot even overcome the power loss through the exhaust channel, as shown in Fig. 5c. The moderate cross section of 60 mm × 40 mm produces the highest net power output among the three designs for most of the operating currents, and only when

Table 9
Pressure drop and power loss through exhaust channels with different baffler angles.

Baffler angle	Pressure drop Δp (Pa)	Power loss P_l (W)
Empty	45.0	1.5
$\beta = 10°$	67.7	2.3
$\beta = 20°$	113.4	3.8
$\beta = 30°$	251.8	8.5
$\beta = 40°$	675.2	22.8

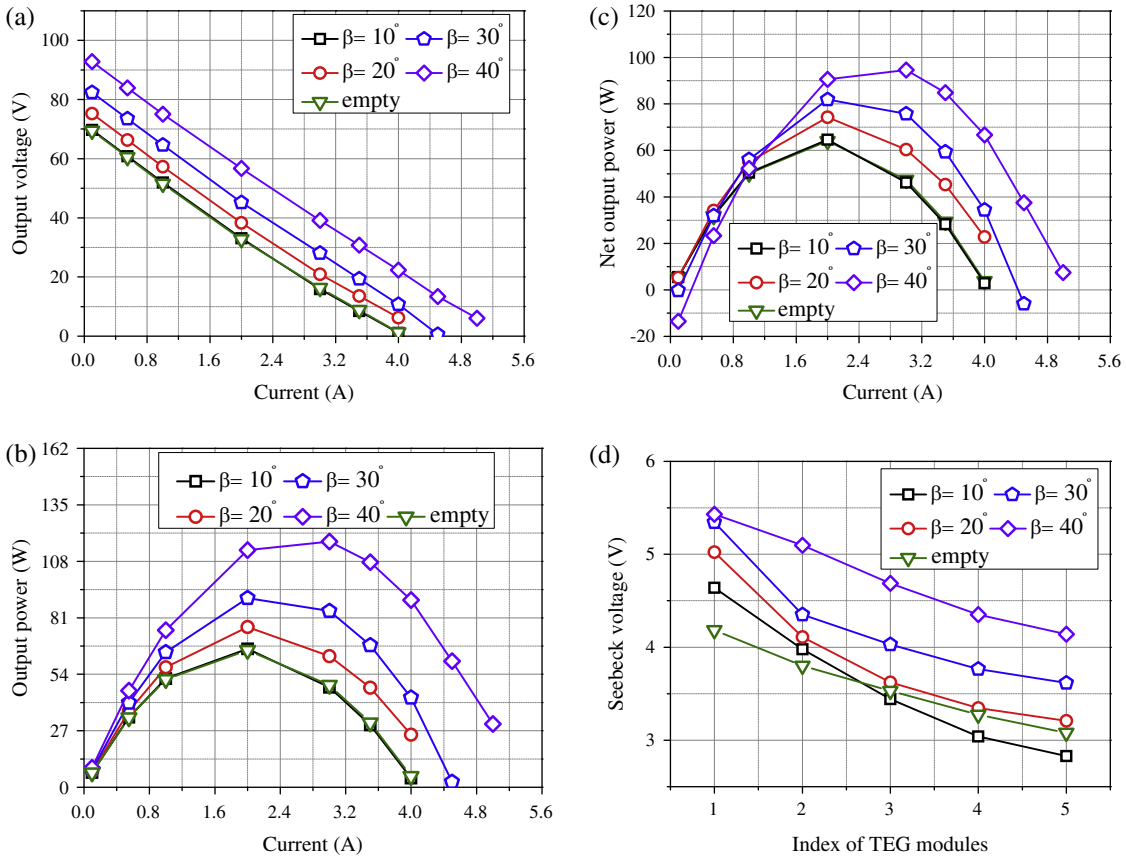

Fig. 14. Change of output voltage (a), power (b) and net power (c) with current, and Seebeck voltages of different TEG modules at 0.1 A (d) for the ETEG systems with different baffler angles.

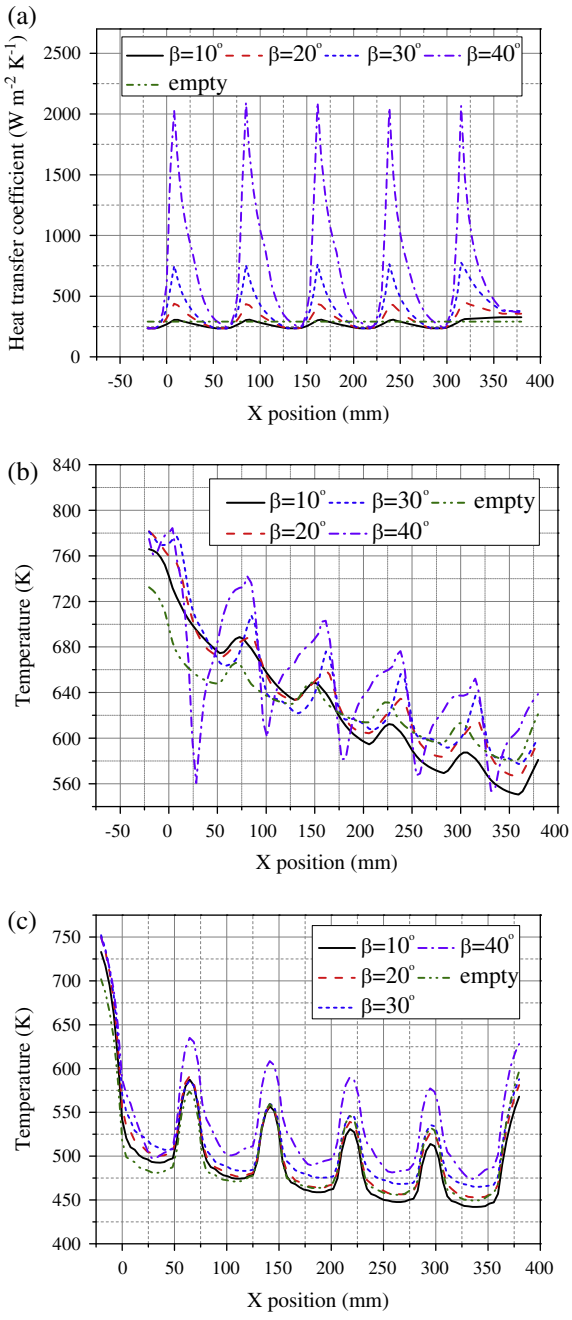

Fig. 15. Heat transfer coefficient (a), gas temperature (middle of exhaust channel and 1 mm from channel wall) (b), and wall temperature (middle of exhaust channel) (c) along the flow direction (*X*-direction) in exhaust channel with different baffler angles.

the current is low (less than 1.3 A), the largest cross section of 120 mm × 40 mm produces the highest net output power.

Therefore, the exhaust channel with the cross section of 60 mm × 40 mm might be considered to balance the flow resistance of the TEG power output, and this cross section is used for the rest of the simulations in this study.

3.2. Effect of number of exhaust channels

As mentioned previously, the ICE considered in this study is a six-cylinder diesel engine. Since high flow rates in exhaust channel may cause large pressure drops, in this study, one, two and three exhaust channels (L = 1, 2, 3) are considered to only provide the flow path for the exhaust from one cylinder, corresponding to one-sixth of the exhaust flow of the six-cylinder engine.

Based on the base operating condition (Case 2 in Table 1), the cases for one, two and three exhaust channels (L = 1, 2, 3) to provide the flow path of the exhaust from one cylinder are studied. In fact, the only difference of the simulation cases with different numbers of exhaust channels (L) is the velocity at the inlet of exhaust channel. Fig. 6 shows the change of voltage, power and net power with current for each exhaust channel and for all the exhaust channels. If the average voltage/power of the exhaust channels for the cases with two and three channels are used for comparison (Fig. 6a–c), the single-exhaust channel case shows both the highest power and net power, and they decrease with more exhaust channels. For example, at 3 A, the average voltages are 50.6 V, 28.7 V and 16.3 V for one, two and three channels, respectively. The average voltage of the single-channel case is about 3 times of the three-channel case. With more exhaust channels, the peak power is produced at lower current, suggesting that increasing the number of channels reduces the performance of each TEG. However, in considering the power loss in exhaust channel in Table 6, it is much lower for the three-channel case than the single-channel.

As a result, Fig. 6d–f shows that the three-channel case produces both the highest TEG power and net power, especially for the net power. It can also be noticed that the improvement in total net power by increasing the number of exhaust channels becomes less significant with more channels. In addition, with more exhaust channels, the current corresponding to peak power decreases. Therefore, properly increasing the number of exhaust channels may improve the ETEG performance, however, since more space and TEG modules are needed, the system size and cost need to be considered as well. It is also suggested that corresponding to different engine operating conditions (exhaust flow rates), making the number of channels adjustable may further improve the ETEG performance.

The results in Sections 3.1 and 3.2 show that the size and shape of exhaust channel may affect ETEG performance significantly, and proper channel design is of paramount importance, because the heat transfer rate from exhaust to TEG and the pressure drop through exhaust channel change significantly with channel design.

3.3. Effect of number of bafflers

In this section, the influence of number of bafflers mounted in exhaust channel is investigated. The bafflers are mounted to enhance the heat transfer to the TEG modules. The number of baffler, defined as N, ranges from 0 to 6 per channel. The dimension of each baffler is 158 mm × 20 mm × 1 mm, along the X-, Y- and Z-directions, respectively. The angle between the channel wall and the baffler, β, is 20°. All the bafflers are evenly spaced in the exhaust channel. A detailed schematic of the exhaust channel with different numbers of bafflers is shown in Fig. 7. The empty exhaust channel without baffler is considered as the base case for comparison. For consistent comparison, except the bafflers, all the other design and operating parameters are kept the same for the simulations in this section.

It can be observed in Fig. 8a–c that the voltage decreases almost linearly as the current increases for all the cases, and the power and net power all follow the increasing–decreasing trend. The peak output power is obtained at about 2 A for all the cases. With one baffler mounted at the inlet, the net power is the lowest, and only when the number of bafflers becomes more than 3, the net power is higher than the empty channel case. As shown in Fig. 8d, for the Seebeck voltages of the five TEG modules, with one baffler at the inlet, the Seebeck voltage of TEG 1 is increased, however, it is even lower than the empty channel case for TEGs 2–5. With more

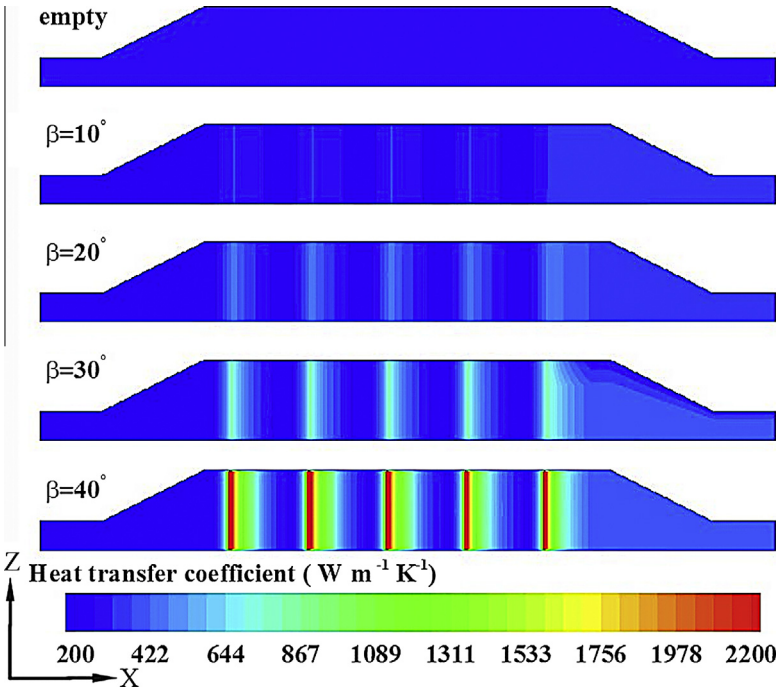

Fig. 16. Contour of heat transfer coefficient for the exhaust channel walls (only half wall is shown) with TEG modules for different baffler angles.

bafflers mounted, the Seebeck voltages of the TEG modules downstream are increased.

The ranges of *X*-coordinate of the five TEG modules (Fig. 2) are given in Table 7, showing that TEGs 1–5 are mounted along the flow direction. Although more bafflers improve the performance, the pressure drop along the exhaust channel increases as well, as shown in Table 8 with an almost linear relationship. Since the results in Fig. 8 suggest that bafflers need to be placed in the whole channel to ensure the performance of all the TEG modules, using five bafflers rather than six corresponding to the five TEG modules rather than six, and placing the five bafflers just before the five TEG modules (the "*N* = 5 im" case) shows similar net power (Fig. 8) and lower pressure drop (Table 8) than the six-baffler case.

To understand the effect of number of bafflers shown in Fig. 8, the heat transfer coefficient (defined in Eq. (14)) and the temperatures of gas near channel wall and wall along the flow direction (*X*-direction) in exhaust channel with different numbers of bafflers are shown in Fig. 9. The exhaust gas temperature shown in this figure is in the middle of the channel, along the line 1 mm away from the channel wall with the TEG modules, and the wall temperature is along the middle line of the wall with the TEG modules. It can be noticed that the heat transfer coefficient (Fig. 9a) is greatly enhanced at the locations with bafflers, and keeps almost constant at the locations without bafflers. Even only with one baffler at the inlet, the heat transfer coefficient is enhanced for the whole channel compared with the empty channel case. However, the near wall gas temperature (Fig. 9b) decreases more significantly than the empty channel case for the whole channel. As a result, compared with the empty channel case, the near wall exhaust gas temperature is only higher at the first TEG module, but lower downstream. Correspondingly, the wall temperature changes with the near wall exhaust gas temperature, influencing the performance of the TEG modules.

The reason is that with only one baffler at the inlet, although the flow velocity is enhanced near the wall, only part of the hot exhaust gas is guided to the near wall region. As a result, after the heat is absorbed by the first TEG module, the near wall exhaust gas temperature becomes much lower than the exhaust gas temperature in the middle of the channel. As shown in Fig. 10a, the empty channel case shows more evenly distributed temperature than the one baffler case, and with more bafflers downstream, more hot exhaust gases are forced to flow to the near wall region, improving both the heat transfer coefficient and near wall exhaust gas temperature. Correspondingly, the near wall temperature shown in Fig. 10b shows the similar trend. Moreover, since the bafflers installed fully covers the exhaust channel along the *Z*-direction, the heat transfer coefficient only changes along the flow direction (*X*-direction), and the change along the *Z*-direction is insignificant (Fig. 11). In addition, the velocity magnitude contours shown in Fig. 12 further confirm the baffler effect on the gas flow in exhaust channel.

The results in this section suggest that to enhance the heat transfer from exhaust channel to TEG modules, bafflers need to be placed at all the locations with TEG modules. Although only placing bafflers at the channel inlet could increase the heat transfer coefficient for the whole channel, the near wall temperature downstream might decrease significantly, leading to performance degradation of the TEG modules downstream. If bafflers can be placed properly according to the locations of the TEG modules, further increasing the number of bafflers may not improve the TEG performance significantly, but further increase the pressure drop along channel. For example, for the ETEG system considered in this study, it is suggested to place one baffler just before each TEG module.

3.4. Effect of baffler angle

In this section, the effect of the angle between baffler and bottom wall of exhaust channel is investigated, which is defined as β, as shown in Fig. 13. Based on the improved exhaust channel of "*N* = 5 im" obtained in Section 3.3, four kinds of exhaust channels with different baffler angles are considered (Fig. 13). The empty exhaust channel without baffler is considered as well for comparison. For consistent comparison, except the bafflers, all the other design and operating parameters are kept the same for the simulations in this section.

An obvious improvement of the output voltage and power is observed as the baffler angle increases, as shown in Fig. 14a and b. Taking the current of 0.1 A as an example, the output voltages

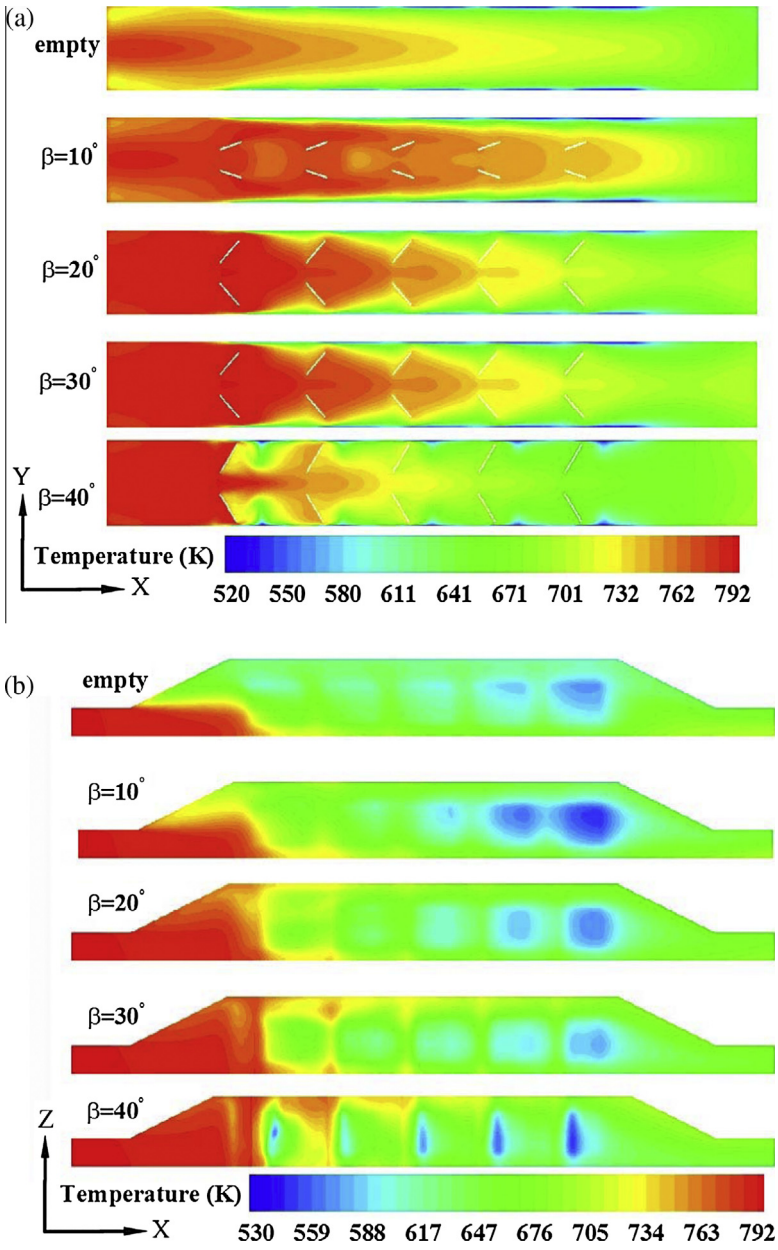

Fig. 17. Contours of temperature in the middle planes of the exhaust channels (a), and near the channel walls (only half wall is shown) with TEG modules (b) for different baffler angles.

of the empty channel, baffler angles of 10°, 20°, 30° and 40° are 69.4 V, 69.7 V, 75.2 V, 82.4 V and 92.8 V, respectively. The percentages of improvement compared with the empty channel case are 0.4%, 8.4%, 18.7% and 33.7%, respectively. Although Table 9 shows that the pressure drop is significantly increased with the increment of baffler angle, especially from 30° to 40°, the net power is still the highest for the angle of 40°, as shown in Fig. 14c. With the smallest angle of 10° shown in Fig. 14d, the Seebeck voltages at 0.1 A of the first three TEG modules are improved compared with the empty channel case, however, the last two TEG modules have lower Seebeck voltages with bafflers. The reason is that with enhanced heat transfer at the inlet of channel, more downstream hot gas needs to be guided to flow to the near wall region, and the angle of 10° is not sufficient for that purpose. The heat transfer coefficient and temperature shown in Fig. 15 confirm that although heat transfer coefficient is improved even with the baffler angle of 10°, the near wall gas temperature downstream becomes lower than the empty channel case, suggesting that the baffler angle needs to be sufficiently high to ensure the near wall gas temperature. With a higher baffler angle, near wall gas temperature variation along the channel becomes more significant, with the trend that the temperature decreases due to the TEG module heat absorption, and increases because the baffler guide more hot gas flowing to the near wall region.

Fig. 16 shows that the heat transfer coefficient is almost evenly distributed for the empty channel case, and with the increment of baffler angle, the heat transfer coefficient becomes more unevenly distributed. Compared by the empty channel case, Fig. 17 shows that the baffler angle of 10° results in more evenly distributed temperature along the *Y*-direction, and by further increasing the baffler angle, more hot gas in the middle is able to flow to the near wall region, the temperature becomes more evenly distributed along the *Y*-direction and higher near the wall, leading to improved performance of the TEG modules. The velocity magnitude distribution shown in Fig. 18 confirms the improvement of heat transfer coefficient with larger baffler angles. With larger baffler angles, it

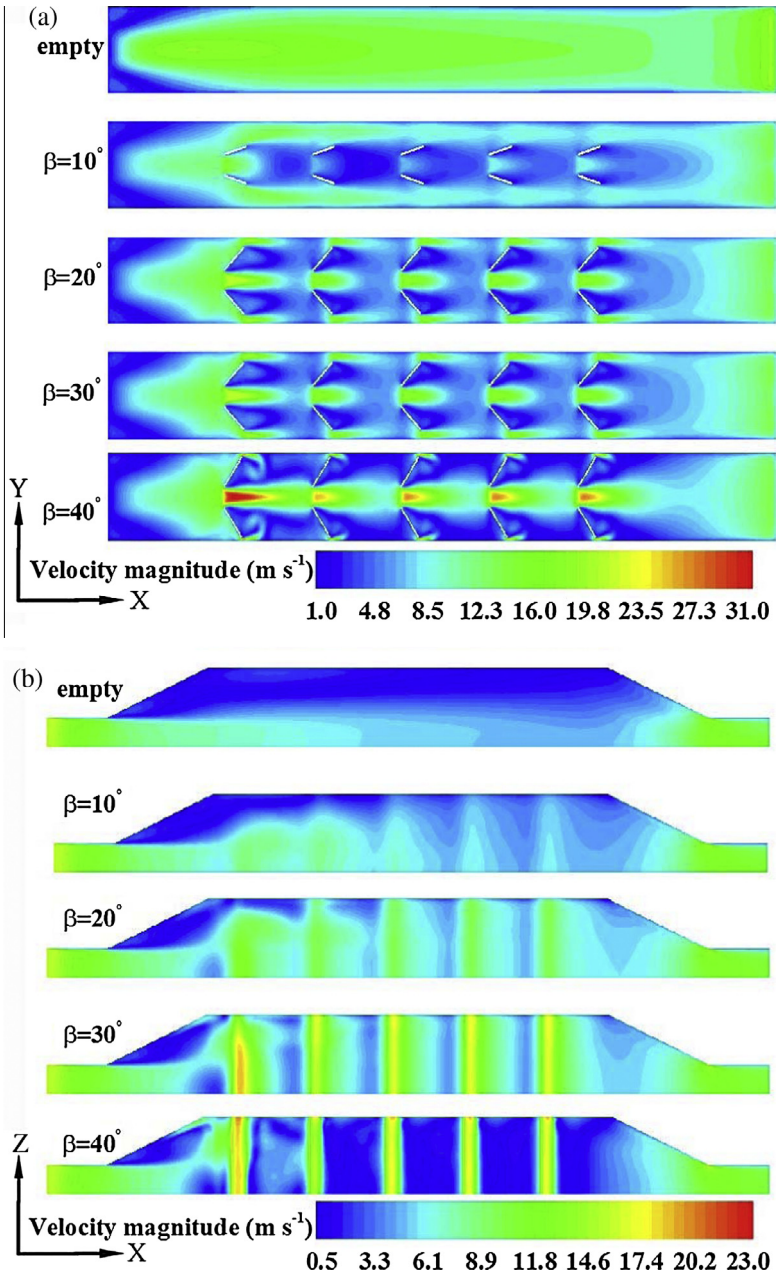

Fig. 18. Contours of velocity magnitude in the middle planes of the exhaust channels (a), and near the channel walls (only half wall is shown) with TEG modules (b) for different baffler angles.

can also be noticed that the velocity magnitude is significantly increased, which is the reason of the high pressure drop in Table 9.

To further assess the performance of the ETEG system, two kinds of efficiency are calculated. One is the efficiency of TEG:

$$\eta_{TEG} = \frac{P_n}{Q_{TEG}} \times 100\% \tag{20}$$

where Q_{TEG} (W) is the heat transfer rate into the hot side of TEG, and P_n (kW) is the net power output of ETEG system. Another one is the efficiency of exhaust waste heat recovery:

$$\eta_{ext} = \frac{P_n}{Q_{ext}} \times 100\% \tag{21}$$

where Q_{ext} (W) is the heat removal rate from engine carried by exhaust gas (only part of this heat can transfer into the hot side of TEG). The reduction of engine fuel consumption by using ETEG system can also be estimated:

$$B_{red} = \frac{B_{ICE}}{P_{ICE}} P_n \tag{22}$$

where P_{ICE} (kW) is the engine power output (Table 1), and B_{ICE} (kg h^{-1}) is the engine fuel consumption rate (Table 1).

Fig. 19 shows the reduction of fuel consumption rate per cylinder, waste heat recovery efficiency of exhaust gas, and efficiency of TEG modules at different operating currents of the TEG modules with the baffler angle (β) of 30°. Taking 2 A as an optimal example, the reduction of fuel consumption rate per cylinder, waste heat recovery efficiency of exhaust gas and efficiency of TEG modules are about 50 g h^{-1}, 1% and 4%, respectively. For the six-cylinder engine, the total reduction of fuel consumption rate is therefore about 0.3 kg h^{-1}, meaning that the fuel consumption rate of the engine is reduced by about 0.6% by using the ETEG system for waste heat recovery. By comparing the waste heat recovery efficiency of exhaust gas (1%) and efficiency of TEG modules (4%), it

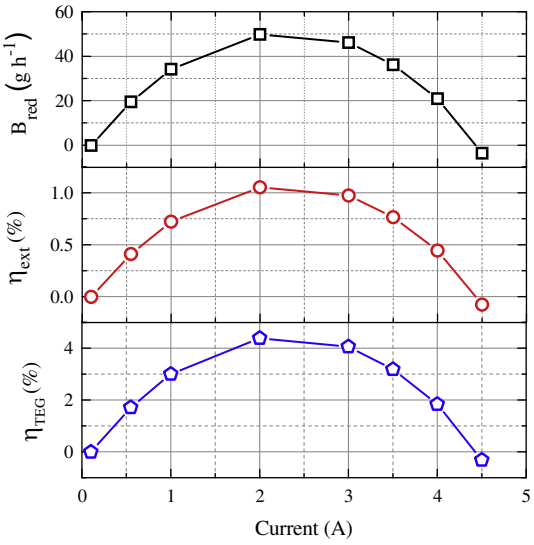

Fig. 19. Reduction of fuel consumption rate per cylinder, waste heat recovery efficiency of exhaust gas, and efficiency of TEG modules at different operating currents of the TEG modules with the baffler angle (β) of 30°.

can be found that only about 25% of the waste heat in exhaust gas is transferred into the TEG modules, suggesting that there is still a significant potential to improve the performance of ETEG system by heat transfer enhancement.

The results in this section suggest that to ensure effective utilization of all the hot exhaust gas, the baffler angle needs to be sufficiently high, especially for the downstream locations. However, higher baffler angles increase the pressure drop significantly, therefore, it is suggested that variable baffler angles, with the angle increasing along the flow direction, might be a middle course for balancing the heat transfer and pressure drop.

3.5. Effect of engine operating condition

In this section, the effect of the different engine operating conditions shown in Table 1 is investigated. According to the results in Section 3.4, the baffler angle of 30° is considered in this section, because this angle could better balance the heat transfer and pressure drop. With the different engine operating conditions, the variable material properties of the p/n semiconductors in Table 3 are used in the simulations. The four operating conditions in Table 1 all correspond to the engine speed of 1500 rpm, and the main difference is the power output. From Cases 1 to 4, the output power is decreased from 258.3 kW to 117.7 kW. For consistent comparison, except the engine operating condition, all the other design and operating parameters are kept the same for the simulations in this section. Fig. 20a and b shows that the output voltage and power of the ETEG system decrease from Case 1 to Case 4, i.e. decease with increment of engine power. Taking the current of 0.5 A as an example, the output powers for Cases 1–4 are 23.9 W, 22.4 W, 18.3 W and 13.1 W, respectively. The main reason is the higher exhaust gas temperature and flow rate with higher engine output power, as shown in Table 1. However, in considering the pressure drop in exhaust channel (Table 10), Case 2 produces the highest net power. The results suggest that a single ETEG design may not be suitable to the various engine operating conditions, and making the number of exhaust channels and baffler angle adjustable according to different engine operating conditions, as suggested in Sections 3.2 and 3.4, might be able to further improve the performance.

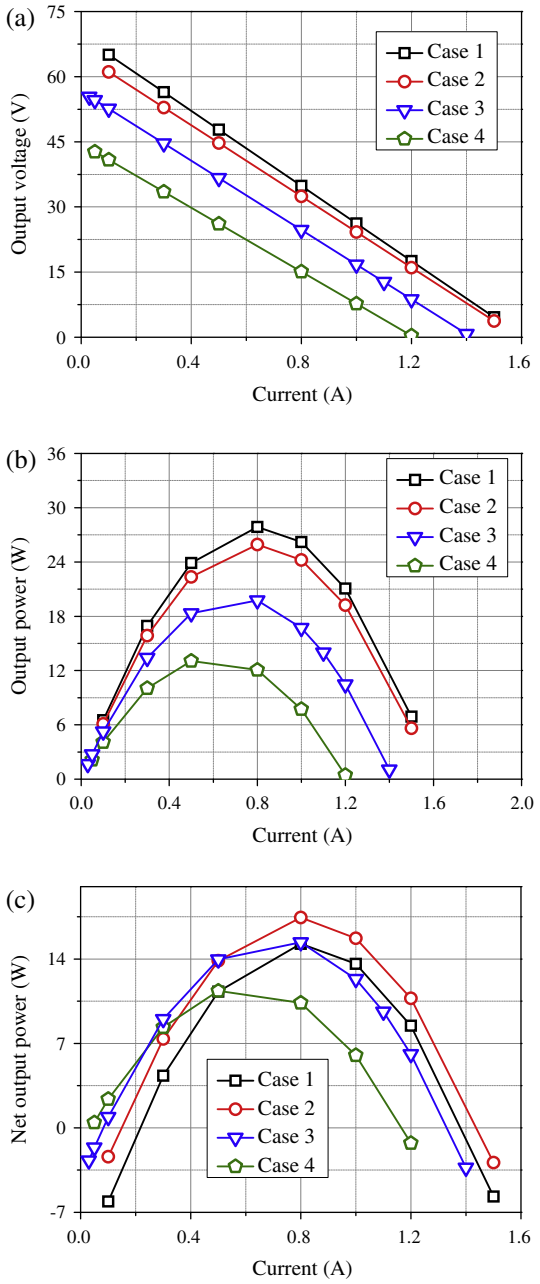

Fig. 20. Change of output voltage (a), power (b) and net power (c) with current for the ETEG system with different engine operating conditions (Table 1).

Table 10
Pressure drop and power loss through exhaust channels with different engine operating conditions (Table 1).

Case	Inlet velocity v_{in} (m s^{-1})	Pressure drop Δp (Pa)	Power loss P_l (W)
1	17.4	327.4	12.6
2	15.3	251.8	8.5
3	11.9	165.7	4.4
4	8.4	90.3	1.7

4. Conclusion

In this study, a 3-D numerical model for exhaust-based thermoelectric generator (ETEG) system has been developed. The effects of exhaust channel size, number of channel, number of baffler, baffler angle and engine operating condition on the heat, mass and

electric transfer characteristics and performance of ETEG are investigated in details. By considering the detailed geometry of the thermoelectric generator (TEG) and exhaust channel as the computational domain, various transport phenomena are observed and elucidated. Suggestions on design optimization are given based on the numerical results. It is found that a smaller inlet of exhaust channel enhances the heat transfer to TEG modules, but increases the flow resistance, and therefore a moderate channel size is needed. Based on the design and operating conditions in this study, the exhaust channel with the cross section of 60 mm × 40 mm might be optimal to balance the flow resistance and TEG power output. Increasing the number of exhaust channels may improve the ETEG performance, however, since more space and TEG modules are needed, the system size and cost need to be considered as well. With multiple channels per cylinder, it is also recommended to make the number of working channels adjustable for further performance improvement. To enhance the heat transfer from exhaust channel to TEG modules, bafflers need to be placed near all the TEG modules. Although only placing bafflers at the channel inlet could increase the heat transfer coefficient for the whole channel, the near wall temperature downstream might decrease significantly, leading to performance degradation of the TEG modules downstream. If bafflers can be placed properly according to the locations of the TEG modules, further increasing the number of bafflers may not improve the TEG performance significantly, but increase the pressure drop along channel. For example, for the ETEG system considered in this study, it is suggested to place one baffler just before each TEG module. To ensure effective utilization of the hot exhaust gas, the baffler angle needs to be sufficiently large, especially for the downstream locations. However, larger baffler angles increase the pressure drop significantly, therefore, it is suggested that variable baffler angles, with the angle increasing along the flow direction, might be a middle course for balancing the heat transfer and pressure drop. For the six-cylinder engine and ETEG system in this study, the total reduction of fuel consumption rate can reach about 0.3 kg h^{-1}, meaning that the fuel consumption rate of the engine is reduced by about 0.6% by using the ETEG system for waste heat recovery. By comparing the waste heat recovery efficiency of exhaust gas (1%) and efficiency of TEG modules (4%), it can be found that only about 25% of the waste heat in exhaust gas is transferred into the TEG modules, suggesting that there is still a significant potential to improve the performance of ETEG system by heat transfer enhancement. A single ETEG design may not be suitable to the various engine operating conditions, and making the number of exhaust channels and baffler angle adjustable according to different engine operating conditions might be able to further improve the performance.

Acknowledgements

This research is supported by the National Basic Research Program of China (973 Program, No. 2011CB707201), the National Natural Science Foundation of China (Grant No. 51276121) and High Performance Computing Center of Tianjin University, China.

References

[1] Stabler F. Automotive applications of high efficiency thermoelectrics. DARPA/ONR Program Review and DOE High efficiency Thermoelectric Workshop, San Diego, CA, March 24–27; 2002.
[2] Vazquez J, Sanz-Bobi M, Palacios R, Arenas A. State of the art of thermoelectric generators based on heat recovered from the exhaustes of autombiles. In: Proceedings of the seventh European workshop on thermoelectrics; 2002.
[3] LaGrandeur J, Crane D, Hung S, Mazar B, Eder A. Automotive waste heat conversion to electric power using skutterudite, TAGS, PbTe and BiTe. In: International conference on thermoelectrics; 2006. p. 343–48.
[4] Thacher EF, Helenbrook BT, Karri MA, Richter CJ. Testing of an automobile exhaust thermoelectric generator in a light truck. Proc Inst Mech Eng D: J Automob Eng 2007;221:95–107.
[5] Hsu CT, Huang GY, Chu HS, Yu B, Yao DJ. Experiments and simulations on low-temperature waste heat harvesting system by thermoelectric power generators. Appl Energy 2011;88:1291–7.
[6] Saqr KM, Mansour MK, Musa MN. Thermal design of automobile exhaust based thermoelectric generators: objectives and challenges. J Thermoelect 2008;1:59–66.
[7] André C, Vasilevskiy D, Turenne S, Masut RA. Extruded bismuth–telluride based n-type alloys for waste heat thermoelectric recovery applications. J Electron Mater 2009;38(2009):; 1061–1067.
[8] Hadjistassou C, Kyriakides E, Georgiou J. Designing high efficiency segmented thermoelectric generators. Energy Convers Manage 2013;66:165–72.
[9] Vikhor LN, Anatychuk LI. Generator modules of segmented thermoelements. Energy Convers Manage 2009;50:2366–72.
[10] El-Genk MS, Saber HH. High efficiency segmented thermoelectric unicouple for operation between 973 and 300 K. Energy Convers Manage 2003;44:1069–88.
[11] Saber HH, El-Genk MS. Effects of metallic coating on the performance of skutterudite-based segmented unicouples. Energy Convers Manage 2007;48:1383–400.
[12] Butt S, Ren YY, Farooq MY, Zhan B, Sagar RUR, Lin YH, et al. Enhanced thermoelectric performance of heavy-metals (M: Ba, Pb) doped misfit-layered ceramics: $(Ca_{2-x}M_xCoO_3)_{0.62}(CoO_2)$. Energy Convers Manage 2014;83:35–41.
[13] Reddy BVK, Barry M, Li J, Chyu MK. Thermoelectric-hydraulic performance of a multistage integrated thermoelectric power generator. Energy Convers Manage 2014;77:458–68.
[14] Sahin A, Yilbas BS. The thermoelement as thermoelectric power generator: effect of leg geometry on the efficiency and power generation. Energy Convers Manage 2013;65:26–32.
[15] Zhou SY, Sammakia BG, White B, Borgesen P. Multiscale modeling of thermoelectric generators for the optimized conversion performance. Int J Heat Mass Transf 2013;62:435–44.
[16] Chen WH, Liao CY, Hung CI, Huang WL. Experimental study on the thermoelectric modules for power generation at virious operating conditions. Energy 2012;45:874–81.
[17] Belanger S, Gosselin L. Thermoelectric generator sandwiched in a crossflow heat exchanger with optimal connectivity between modules. Energy Convers Manage 2011;52:2911–8.
[18] Lesage FJ, Sempels ÉV, Lalande-Bertrand N. A study on heat transfer enhancement using exhaust channel inserts for thermoelectric power generation. Energy Convers Manage 2013;75:532–41.
[19] Rezania A, Rosendahl LA, Andreasen SJ. Experimental investigation of thermoelectric power generation versus coolant pumping power in a microchannel heat sink. Int Commun Heat Mass 2012;39:1054–8.
[20] Chen M, Rosendahl LA, Condra TJ, Pedersen JK. Numerical modeling of thermoelectric generators with varying material properties in a circuit simulator. IEEE Trans Energy Convers 2009;24:112–4.
[21] Chen M, Rosendahl LA, Condra T. A three-dimensional numerical model of thermoelectric generators in fluid power systems. Int J Heat Mass Heat Transfer 2011;54:345–55.
[22] Niu ZQ, Yu SH, Li QS, Jiao K, Du Q, Tian H, et al. Elucidating modeling aspects of thermoelectric generator, in submission. Int J Heat Mass Trans (in submission).
[23] Rowe DM, Min G. Evaluation of thermoelectric modules for power generation. J Power Sources 1998;73:193–8.
[24] Yu JL, Zhao H. A numerical model for thermoelectric generator with the parallel-plate heat exchanger. J. Power Source 2007;172:428–34.
[25] Wang YC, Dai CS, Wang XS. Theoretical analysis of a thermoelectric generator using exhaust of vehicles as heat source. Appl Energy 2013;112:1171–80.
[26] Hsiao YY, Chang WC, Chen SL. A mathematic model of thermoelectric module with applications on the waste heat recovery from automobile engine. Energy 2010;35:1447–54.
[27] Weng CC, Huang MJ. A simulation study of automotive waste heat recovery using a thermoelectric power generator. Int J Therm Sci 2013;71:302–9.
[28] Yu GP, Shu GQ, Tian H, Liu LN. Simulation and thermodynamic analysis of a bottoming Organic Rankine Cycle (ORC) of diesel engine (DE). Energy 2013;51:281–90.
[29] Perry RH. Perry's chemical engineers' handbook. 6th ed. New York: McGraw-Hill; 1984.
[30] <http://www.dieselnet.com/tech/diesel_exh.php#intro> (accessed 2014.03.20).
[31] Gou XL, Yang SW, Ou XHQ. A dynamic model for thermoelectric generator applied in waste heat recovery. Energy 2013;52:201–9.
[32] Fraisse G, Ramousse J, Sgorlon D, Goupil C. Comparison of different modeling approaches for thermoelectric elements. Energy Convers Manage 2013;65:351–6.
[33] Fluent user's guide.
[34] Yang YS, Tao WQ. Heat transfer. 4th ed. Higher Education Press; 2006.
[35] Jang JY, Tsai YC, Wu CW. A study of 3-D numerical simulation and comparison with experimental results on turbulent flow of venting flue gas using thermoelectric generator modules and plate fin heat sink. Energy 2013;53:270–81.
[36] Hsu CT, Huang GY, Chu HS, Yu B, Yao DJ. An effective Seebeck coefficient obtained by experimental results of a thermoelectric generator module. Appl Energy 2011;88:5173–9.